Attenuated Total Reflection Fourier Transform Infrared Studies of Redox Changes in Bovine Cytochrome *c* Oxidase: Resolution of the Redox Fourier Transform Infrared Difference Spectrum of Heme a_3[†]

Peter R. Rich*[,‡] and Jacques Breton[§]

Glynn Laboratory of Bioenergetics, Department of Biology, University College London, Gower Street, London WC1E 6BT, United Kingdom, and Section de Bioénergétique, Département de Biologie Cellulaire et Moléculaire, Bât. 532, CEA-Saclay, 91191 Gif-sur-Yvette Cedex, France

Received May 11, 2001; Revised Manuscript Received October 22, 2001

ABSTRACT: Attenuated total reflection Fourier transform infrared (ATR-FTIR) difference spectroscopy has been performed on samples of bovine cytochrome *c* oxidase that have been deposited as a thin film on the surface of a silicon microprism. The technique has several advantages over transmission methods in terms of amount of material required, the time required to reach sufficient optical stability, and the range of reactants that can be repetitively added and removed. The ATR-FTIR method has been used to record redox difference spectra of cytochrome *c* oxidase in the unligated and cyanide-ligated states. By subtraction of the spectra, the redox FTIR difference spectrum of heme a_3 can be resolved from those of the other metal centers. This difference spectrum is compared with available vibrational and Raman data on homologous oxidases and on heme A model compounds.

Fourier transform infrared (FTIR)[1] spectroscopy may be used to probe changes in individual cofactors and amino acids in proteins caused by ligand binding and protonation changes. The transmission technique has been applied to cytochrome *c* oxidase to monitor changes induced by photolysis of ligands (*1*−*11*) or by oxidation/reduction (*12*−*17*). These measurements require concentrated samples of protein sealed within a pair of IR-transparent optical windows, and changes are initiated photochemically or electrochemically. Valuable information has been obtained on modes of ligand binding, on amino acid and prosthetic group changes, and on protonation changes within the protein. Here we describe the extension of attenuated total reflection (ATR) FTIR (*18*) spectroscopy to the study of thin layers of bovine cytochrome *c* oxidase that have been deposited on the surface of a silicon microprism. The apparatus allows measurement of changes in the infrared spectrum of the protein film while an aqueous solution flows continuously over its exposed surface (Figure 1). ATR-FTIR spectroscopy has already been applied to several proteins including rhodopsin, bacteriorhodopsin, and the nicotinic acetylcholine receptor (*18*), and it greatly extends the types of transitions that can be analyzed by FTIR spectroscopy. The ATR-FTIR method has been used here to generate redox difference spectra of the unligated and cyanide-bound states of bovine cytochrome *c* oxidase. The difference between these spectra provides a means of resolution of the redox FTIR difference spectrum of heme a_3 from those of the other metal centers.

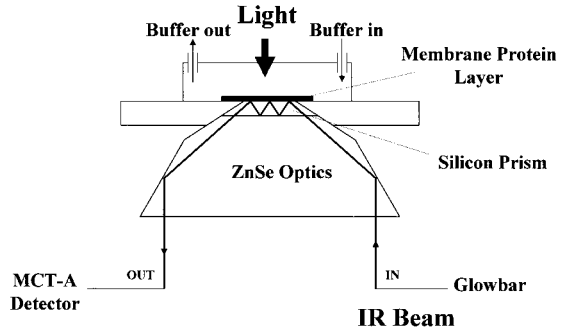

FIGURE 1: ATR-FTIR apparatus. The ATR device (SensIR Technologies) consists of a silicon microprism mounted in a stainless steel plate such that a 3 mm diameter surface is exposed for sample application. The IR beam is deflected into and out of the prism by zinc selenide optics, and the geometry is such that three internal reflections occur at the prism surface on which the sample is attached. After sample attachment (see Figure 2), a Perspex chamber is attached so that buffer can be flowed continuously over the exposed protein film. For photolytic spectra, a light pipe directed over the sample delivers actinic visible light.

MATERIALS AND METHODS

Preparation of Bovine Cytochrome c Oxidase Samples. Cytochrome *c* oxidase was prepared from beef heart by a procedure (*19*) that yields "fast" enzyme with monophasic cyanide binding kinetics and a characteristic Soret maximum at 424 nm. The final preparation was dissolved in 0.1 M potassium phosphate, 0.1 M potassium borate, and 0.1% (w/v) Tween-80, pH 8.5, to a concentration of 150−350 μM, as quantitated from the dithionite-reduced minus oxidized optical difference spectrum by use of an extinction coefficient

[†] This work was funded by grants from the Wellcome Trust (Grant 062827) and the French and British Councils (Franco British Alliance Joint Research Program, Project PN 98.009).

* To whom correspondence should be addressed: Tel/fax (+44) 020 7679 7746; e-mail PRR@UCL.AC.UK.

[‡] University College London.

[§] CEA-Saclay.

[1] Abbreviations: (ATR) FTIR spectroscopy, (attenuated total reflection) Fourier transform infrared spectroscopy; CO, carbon monoxide; DAD, 2,3,5,6-tetramethyl-*p*-phenylenediamine; PMS, phenazine methosulfate.

10.1021/bi0109717 CCC: $22.00
Published on Web 12/22/2001

of $\Delta\epsilon_{606-621nm} = 25.7\ mM^{-1}\ cm^{-1}$ (*20*). Aliquots were stored in liquid nitrogen until required.

Preparation and Measurement of ATR-FTIR Samples. Stable association between protein and the prism surface in the wet state relies on hydrophobic interactions. To achieve large, stable, and reproducible protein signals, both protein sample and crystal surface require pretreatment. Detergent depletion of the oxidase was achieved by dilution into 30−300 volumes of 0.1% (w/v) sodium cholate in a buffer of 50 mM potassium phosphate at pH 8.5. The oxidase, which was still soluble at this stage, was pelleted by centrifugation at $100000g_{av}$ for 1 h. The pellet was resuspended with a glass homogenizer in 1 mM potassium phosphate at pH 8.5, at which point it became turbid due to lack of added detergent. The sample was centrifuged at $50000g_{av}$ for 30 min and formed a tight, turbid pellet. This was homogenized into a small amount of 1 mM potassium phosphate buffer at pH 8.5 and used immediately or stored in small aliquots at −80 °C. The silicon microprism surface (SensIR Technologies, three-bounce version, surface diameter 3 mm, see Figure 1) as supplied was hydrophobic and bound detergent-free protein readily. However, with repeated use the prism surface became unreliable, even if washed extensively. Therefore, to give reproducible behavior, the surface was occasionally polished lightly with a paste of 0.03 μm alumina powder in distilled water, washed with distilled water, and dried. The oxidase sample (approximately 150 pmol of detergent-depleted enzyme suspended in 15 μL of 1 mM potassium phosphate at pH 8.5) was placed on the prism surface, dried with a gentle stream of dry air, and then rewetted with 50 mM potassium phosphate at pH 8.5. After rewetting, a Perspex lid was attached that allowed a continuous flow of buffer over the exposed sample surface, driven by a peristaltic pump at a flow rate of 1−2 mL/min.

FTIR spectra were recorded with a Bruker ISF 66/S spectrometer, fitted with a liquid nitrogen-cooled MCT-A detector. All frequencies quoted have an accuracy to ±1 cm^{-1}. Typically, 500 interferograms at 4 cm^{-1} resolution were averaged over a period of around 70 s to provide a background, and spectra versus this background were then recorded. When the sample was sufficiently stable, a new baseline was recorded, the reactant was introduced, and spectra were recorded until the change was complete, usually within 5 min. Four successive FTIR difference spectra were then averaged to provide a final spectrum. The transitions were reversible, and oxidation and reduction could be repeated reproducibly many times without significant change of signal intensity. In a typical run, three oxidative and three reductive transitions were performed and spectra were averaged to provide a final redox difference spectrum. The FTIR difference spectra due to changes of reagent solutions were recorded separately in the absence of protein. These spectra were routinely subtracted from the protein spectra, although changes in the protein region were small in comparison to those of the protein itself.

RESULTS

Formation of a Stable Protein Film. Figure 2 shows the spectroscopic properties of the volume probed by the evanescent wave (*18*) near the prism surface during deposition of the protein sample. When placed initially as an aqueous suspension, the spectrum was essentially only that of water. After drying with a gentle stream of dry air, however, large signals of protein appeared (most prominently seen in Figure 2 as the amide I and II bands at 1650 and 1539 cm^{-1}, respectively), together with signals from lipid and other constituents. When the dried sample was rewetted with 50 mM potassium phosphate at pH 8.5, the water bands reappeared whereas the protein bands decreased uniformly as the protein layer rehydrated. However, the intensities of the protein bands stabilized rapidly. Their level was most easily quantitated from the amide II band measured as a peak (1539 cm^{-1} when dry and 1545 cm^{-1} when rewetted) minus the low-frequency trough at 1481 cm^{-1}, which stabilized at a level of 30−55% of the magnitude of the dry state. The sample drift was generally sufficiently stable after 10−15 min (<0.0001 ΔA/min in the amide I/II region and much less elsewhere) to allow recording of ligand- or redox-induced FTIR difference spectra. A loading of 150 pmol of oxidase was sufficient to produce a maximum protein signal in the rewetted state, and larger amounts were without further effect. If the dimensions for an oxidase monomer are approximated to be 100 Å diameter and 120 Å height (*21*), then its molecular volume is around $0.94 \times 10^{-6}\ \mu^2$ and it may be calculated that the film (deposited diameter of approximately 5 mm so that it contacts the stainless steel prism surround) must have a thickness of at least 4.3 μm, which exceeds the expected depth of penetration of the evanescent wave in this frequency range (*18*).

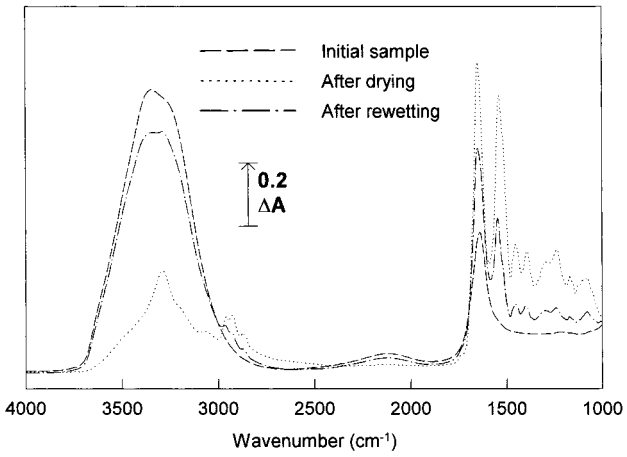

FIGURE 2: Spectroscopic properties of oxidase sample during drying and rewetting on a silicon microprism. A sample of detergent-depleted bovine cytochrome *c* oxidase (approximately 150 pmol in 15 μL of 1 mM potassium phosphate buffer at pH 8.5) was placed on the prism surface and the initial spectrum (− − −) was recorded. The sample was then dried with a gentle stream of dry air. This resulted in a stable spectrum (· · ·) that consisted of prominent protein vibrations, together with a very low amount of water that did not decrease further and presumably arises from tightly bound structural water molecules. After rewetting with 50 mM potassium phosphate at pH 8.5, a spectrum (− · −) stabilized over several minutes in which the protein features diminished by approximately 60% and much of the water spectrum reappeared.

Comparison of Transmission FTIR and ATR-FTIR Spectra. To assess the validity of the spectra produced by the above protocols, a comparison was made of CO photolysis spectra obtained by the transmission and ATR methods. An ATR film of 150 pmol of detergent-depleted oxidase sample was prepared as above. When the film had stabilized with a continuous flow of 50 mM potassium phosphate at pH 8.5,

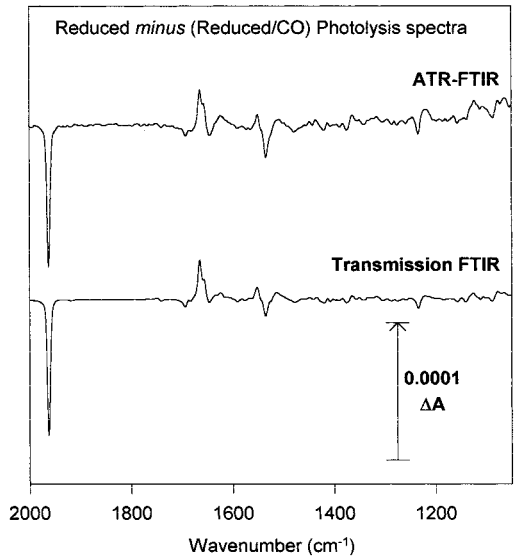

FIGURE 3: Comparison of reduced minus (reduced/CO) photolysis spectra of bovine cytochrome *c* oxidase recorded by ATR-FTIR and transmission FTIR spectroscopy. A rewetted film of 150 pmol of detergent-depleted cytochrome oxidase was attached to the silicon prism and a CO-saturated buffer of 50 mM potassium phosphate at pH 8.5 containing 10 mM sodium dithionite was pumped onto the surface to generate the CO-ligated, fully reduced species as described in the text. Repetitive light/dark cycles were then performed in order to generate a signal-averaged CO photolysis spectrum, as described in ref *22*. The ATR-FTIR photolysis spectrum shown is the average of 1350 individual spectra (each of which is an average of 100 interferograms at 4 cm^{-1} resolution at room temperature). For comparison, an equivalent spectrum is plotted of data obtained previously (*22*) by transmission FTIR (2−3 nmol of oxidase sample; average of 2800 individual spectra, each of which is an average of 100 interferograms at 4 cm^{-1} resolution). The transmission FTIR spectrum has been normalized so that the trough due to photolysis of bound CO is the same in both spectra.

the flow solution was changed to the same buffer containing 5 mM sodium dithionite and saturated with CO. The characteristic 1963 cm^{-1} band of CO bound to ferrous heme a_3, together with bands in the 1800−1000 cm^{-1} region due to reduction of enzyme, formed over several minutes and confirmed the formation of the ferrous−CO adduct of heme a_3. When the 1963 cm^{-1} band had formed fully, the buffer flow was stopped and the sample was subjected to repetitive light/dark photolysis cycles as described previously (*22*) in order to generate a reduced minus (reduced/CO) photolysis spectrum. The resultant averaged spectrum (150 pmol sample at 23 °C; average of 1350 spectra, each of which is an average of 100 interferograms at 4 cm^{-1} resolution) is shown in Figure 3. For comparison, an equivalent spectrum is plotted of data obtained previously (*22*) by transmission FTIR (2−3 nmol of the same oxidase preparation at 12 °C; average of 2800 spectra, each of which is an average of 100 interferograms at 4 cm^{-1} resolution), normalized so that the trough due to photolysis of bound CO is the same in both spectra. All major features of the transmission FTIR spectra are also present in the ATR-FTIR spectrum. The most noticeable difference between the two spectra is an increase in signal intensities of individual features in the ATR-FTIR spectrum as the wavenumber decreases. This effect is due to an increasing depth of penetration of the evanescent wave, which is inversely proportional to frequency (*18*), and leads to a greater path length for low-frequency features in the ATR spectrum. It may be concluded that, provided the

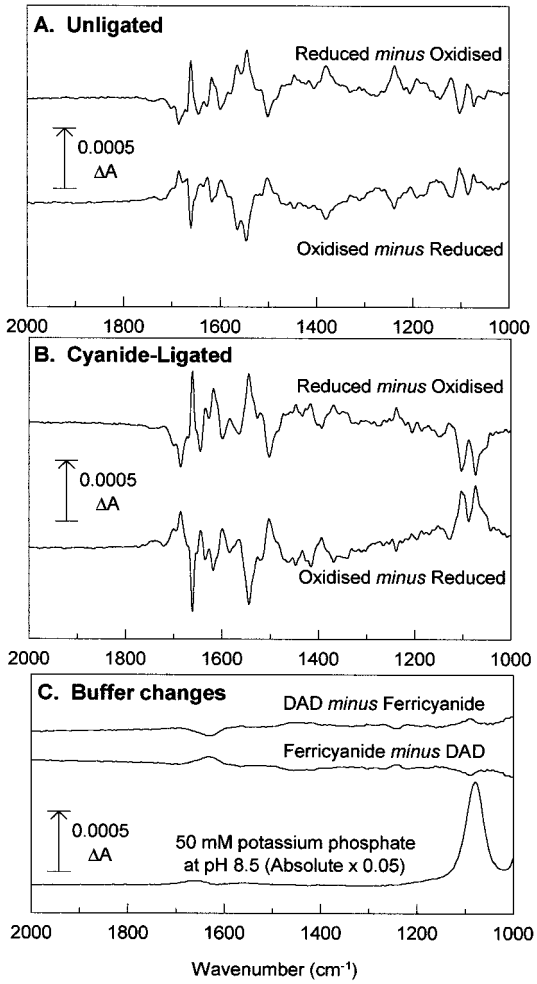

FIGURE 4: ATR-FTIR difference spectra during reduction and oxidation of a rewetted film of cytochrome *c* oxidase in the unligated and cyanide-ligated states. A rewetted film of 150 pmol of detergent-depleted cytochrome oxidase was attached to the silicon prism as in Figure 2 and equilibrated with a continuous flow of 50 mM potassium phosphate buffer at pH 8.5 containing 2 mM potassium ferricyanide and 10 μM PMS. When the spectrum had stabilized, a baseline was recorded and the flow solution was switched to 50 mM potassium phosphate buffer at pH 8.5 containing 2 mM DAD and 2 μM PMS. Spectra (500 interferograms at 4 cm^{-1} resolution) were then recorded until no further change occurred, and four spectra were then averaged to give the final result. The same protocol was repeated when changing back to the ferricyanide-containing buffer. The spectra shown are an average of three reductive and three oxidative cycles. In panel B, the same sample was used after switching to reductive and oxidative buffers as for panel A, but the buffers also contained 2 mM potassium cyanide to generate and maintain the cyanide-ligated form of the enzyme. Panel C shows the changes induced by change of the oxidative and reductive buffers in the absence of protein. The DAD minus ferricyanide spectrum is that induced by replacing the ferricyanide/PMS buffer with that containing DAD/PMS, and the ferricyanide minus DAD spectrum represents the inverse buffer change. Also shown is the absolute spectrum of 50 mM potassium phosphate at pH 8.5 (scaled by a factor of 0.05) after subtraction of the water contribution.

frequency-dependent intensity distortion is taken into account, the ATR-FTIR protocol is producing valid and reproducible spectroscopic data.

Reduced minus Oxidized FTIR Difference Spectra of Unligated and Cyanide-Ligated Cytochrome c Oxidase. Figure 4A shows the spectral changes induced by reduction and reoxidation of a film of cytochrome oxidase on the

silicon prism, induced by alternating flows of 2 mM DAD (a mild reductant) or 2 mM potassium ferricyanide (an oxidant), both of which were dissolved in 50 mM potassium phosphate at pH 8.5 containing 10 μM PMS to mediate redox equilibration with the protein. DAD and ferricyanide were chosen for the redox transitions because they induce full oxidation and reduction of unligated oxidase on reasonable time scales in the presence of PMS as mediator, whereas DAD is not reducing enough to cause reduction of the ferric a_3−cyanide adduct (see below). Furthermore, at the required concentrations none of the compounds cause major contributions in the 2000−1000 cm^{-1} protein/heme region that was the primary interest. Ferricyanide does partially overlap the bands of bound cyanide at 2151 and 2131 cm^{-1} but it could be largely removed by subtraction, as described below, so this did not present a problem in detection of the bound cyanide bands. Large reversible changes occurred in the 1800−1000 cm^{-1} range that can be attributed to redox-induced changes of the protein and prosthetic groups. The reduction/oxidation cycle could be repeated many times in a reproducible manner (little change of signal amplitude was found after 20 cycles). Figure 4A shows averaged reduced minus oxidized and oxidized minus reduced spectra obtained from three reductive and three oxidative cycles of the unligated enzyme and after subtraction of the small changes due to change of buffer reagents (Figure 4C).

The protocol used for redox difference spectra of the unligated enzyme was repeated with the same sample, but with 2 mM KCN added to both oxidant and reductant solutions. On switching from ferricyanide/PMS buffer to the ferricyanide/PMS/KCN buffer, a characteristic 2151 cm^{-1} band due to heme a_3^{3+}−cyanide−Cu_B^{2+} (*1*) formed over a period of several minutes. Cyclic reduction and reoxidation resulted in the averaged reduced minus oxidized and oxidized minus reduced spectra for the cyanide-ligated enzyme shown in Figure 4B (again each an average of three reductive and three oxidative cycles and after subtraction of buffer changes shown in Figure 4C). That the enzyme was cycling between states in which the heme a_3 remained in the ferric and cyanide-ligated states was confirmed by examination of the 2100−2200 cm^{-1} region. This region of the reduced minus oxidized spectrum is shown in Figure 5. The peak/trough in the 2120−2105 cm^{-1} range is a small residue of the very large signal due to ferricyanide that remains after the majority has been removed by subtraction of the baseline due to buffer change alone. However, what can also be reproducibly seen in this reduced minus oxidized difference spectrum is a trough at 2151 cm^{-1} due to loss of heme a_3^{3+}−HCN−Cu_B^{2+} and a positive peak at 2131 cm^{-1} that has been attributed to heme a_3^{3+}−HCN−Cu_B^{1+} (*1*). These two signals are reversed in the equivalent oxidized minus reduced spectrum (not shown), again confirming reversibility of the transition.

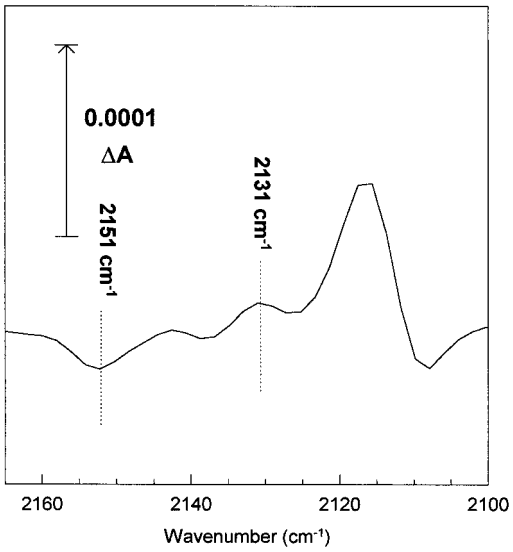

FIGURE 5: ATR-FTIR reduced minus oxidized difference spectrum of a rewetted film of cyanide-ligated cytochrome *c* oxidase in the 2100−2170 cm^{-1} region. The 2100−2170 cm^{-1} region of the reduced minus oxidized spectrum of the cyanide-ligated enzyme from Figure 4B is plotted to show the bound cyanide bands at 2151 and 2131 cm^{-1}.

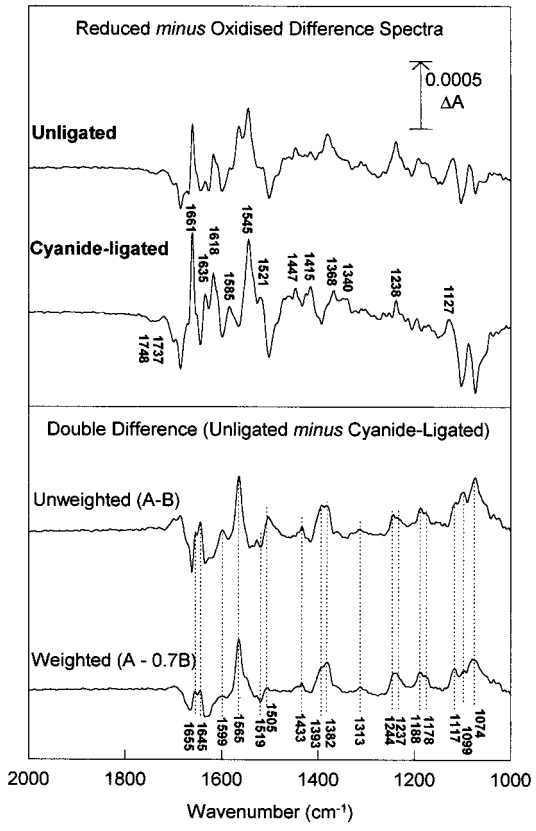

FIGURE 6: Averaged reduced minus oxidized difference spectra of unligated and cyanide-ligated cytochrome *c* oxidase and derived difference spectrum of heme a_3. For the top panel, reduced minus oxidized and oxidized minus reduced spectra of Figure 4 were averaged after inversion of the oxidized minus reduced spectra. The lower panel shows the unligated minus cyanide-ligated double difference spectrum, both as an unweighted subtraction and as a weighted subtraction of 0.7 of the cyanide-ligated spectrum.

DISCUSSION

Deconvolution of the Redox FTIR Difference Spectrum of Heme a_3. In the presence of cyanide, heme a_3 remains in the oxidized, cyanide-ligated state with mild reductants such as DAD ($E_{m7} = +240$ mV), whereas Cu_A, heme *a*, and Cu_B are known to undergo oxidation/reduction readily (*23*). Hence, provided that the redox spectra of these latter three centers are the same in both conditions, the difference between the redox spectra of unligated and cyanide-bound enzyme should represent primarily the redox difference spectrum of heme a_3 alone. In Figure 6, the reduced minus oxidized and oxidized minus reduced spectra of Figure 4

Table 1: Previously Assigned IR and Raman Bands for Ferrous Heme a_3

FTIR data				resonance Raman data	
Paracoccus cyt *c* oxidase[a]		bovine cyt *c* oxidase[b]		bovine cyt *c* oxidase[c]	
cm^{-1}	assignment	cm^{-1}	assignment	cm^{-1}	assignment
1734	Glu 278				
1712	ν(C═O) Asp/Glu				
1694	ν(C═O) Asp/Glu				
1684	amide I (β sheet)				
1662	ν(C═O) a_3 formyl			1662−4	ν(C═O) a_3 formyl
		1655	amide I, ν(C═O) a_3 formyl		
		1645	amide I, ν(C═O) a_3 formyl		
1632	$\nu_s(CN_3H_5^+)$ Arg				
				1622	ν(C−C) a_3 vinyl
1618	ν(C−C) a_3 vinyl				
				1607	ν_{10} a_3 heme
		1599	unassigned		
				1579	ν_2 a_3 heme
		1565	amide II, υ_{37} a_3 heme	1565−9	ν_{37} a_3 heme
1546	ν_{38s} a_3 heme				
1528	heme a_3 propionate ν_{38s} a_3 heme				
				1517	a_3 heme
1512	ring OH Tyr				
		1505	Tyr ring bend		
				1467	a_3 heme
		1433	a_3 heme	1435	a_3 heme
1424	$\nu(COO^-)^s$ Asp/Glu				
		1393	a_3 heme	1389−95	a_3 heme
		1382	a_3 heme		
1362	ν_{41} a_3 heme				
				1355	ν_4 a_3 heme
				1327	a_3 heme
		1313	unassigned		
		1244	a_3 heme	1247	$\nu_5 + \nu_9$ a_3 heme
		1237	a_3 heme	1225	ν_{13} a_3 heme
		1188	unassigned		
		1178	unassigned		
				1129	$\nu_6 + \nu_8$ a_3 heme
		1117	a_3 heme	1115−6	ν_{22} a_3 heme
		1099	possibly His		
		1074	possibly His		

[a] From ref *24*. [b] This work. [c] From refs *28* and *29*.

were first averaged after inversion of the oxidized minus reduced spectra. The figure also shows an unweighted subtraction of the averaged cyanide-ligated reduced minus oxidized spectrum from that of the unligated enzyme. However, the cyanide-ligated spectrum appears to be generally larger than the unligated one throughout the spectrum. This may be a genuine effect due to overlap of opposite signals in the unligated enzyme, or it may arise from a slight contraction of the protein layer in the cyanide-ligated system or from an incomplete reduction of the unligated enzyme during recording. Hence, a weighted subtraction is also shown in Figure 6 in which only 0.7 of the cyanide-ligated enzyme spectrum has been subtracted. Although qualitative differences are apparent, the main features of the spectrum are the same for both subtractions and can be ascribed to the reduced minus oxidized spectrum of heme a_3. Some secondary contributions from the other metal centers might contribute to this spectrum since their own redox difference spectra may vary slightly if heme a_3 is titrating with them, as for the unligated spectrum, or if heme a_3 remains in the ferric, cyanide-ligated state, as is the case for the cyanide-ligated conditions here. However, changes in these metals caused by ligand binding to heme a_3 are likely to be small and, in addition, contributions of the copper centers are likely to appear only in the amide I/II region. Of more concern is the effect of the redox state of heme a_3 on the redox FTIR spectrum of heme *a*, especially since a small shift of the visible spectrum of heme *a* in response to heme a_3 redox state has been reported (*23*). Extension of these studies to include redox transitions of other ligated states of oxidase should clarify the magnitude of such secondary contributions and also allow deconvolution of other individual metal centers.

The overall features of the reduced minus oxidized spectrum of unligated bovine oxidase are similar to, and extend, those obtained electrochemically with transmission FTIR in the 1800−1200 cm^{-1} range (*17*). To date, the only other attempt to separate FTIR redox difference spectra of individual redox components is that of Hellwig et al. (*24*) with the *Paracoccus denitrificans* oxidase. The derived spectrum of *P. denitrificans* heme a_3, however, has little resemblance to the bovine heme a_3 spectrum derived in Figure 6, as can be seen from Table 1, which lists the positions of major features attributed to ferrous heme a_3. The lack of resemblance is unexpected given the high homology between these oxidases in the region of the binuclear center, the general similarity of the overall reduced minus oxidized FTIR difference spectra (*17*), and the roughly comparable Raman data on the heme groups (*25*). However, the redox titration behavior of *Paracoccus* oxidase is reported to be

radically different from that of bovine oxidase: whereas heme *a*, heme a_3, and Cu_B are roughly isopotential and, due to redox interactions, titrate together in a broad redox wave in bovine oxidase, hemes *a* and a_3 appear to titrate as distinct $n = 1$ waves with heme *a* 190 mV higher than heme a_3 in *Paracoccus* oxidase. Furthermore, pH dependency of CO binding frequencies in the *Paracoccus* enzyme indicates an influence of a titratable group within its binuclear center (*9*), whereas an equivalent group is absent in the bovine enzyme (*5*, *10*, *22*). Given such radically different behavior, there is less reason to expect the redox difference spectra of heme a_3 to be comparable in the two types of oxidase.

Comparison can also be made with the published resonance Raman data on model heme A compounds (*26*) and on bovine cytochrome *c* oxidase (*27*−*29*), and in this case the similarities are more extensive (Table 1). Such comparison suggests that many of the most prominent features of the heme a_3 redox difference spectrum in Figure 6 are likely to arise from shifts of heme a_3 porphyrin vibrations. Hence, peaks and troughs in the 1670−1620 cm^{-1} region may be attributed to redox-induced changes in ν(C═O) of the heme a_3 formyl group, changes in the 1720−1680 cm^{-1} region to heme a_3 propionate groups (*30*), and peaks/troughs in the 1430, 1240, and 1120 cm^{-1} regions due to porphyrin and vinyl modes are expected from differences of reduced and oxidized Raman spectra of formyl-heme A (*26*) and of hemes a/a_3 (*28*). Amide I/II contributions from surrounding protein are limited, suggesting a significant rigidity in the protein region around heme a_3 and consistent with a net electroneutral charge change on reduction (*31*). However, some contributions of amide I changes in the 1690−1620 cm^{-1} region may be expected to overlap the changes in ν(C═O) of the heme a_3 formyl group, and the large band at 1565 cm^{-1}, which might be used as a marker to distinguish the redox difference spectrum of heme a_3 from that of heme *a*, presumably arises from amide II band changes. Changes in the 1100−1000 cm^{-1} region may be distorted by small changes in the large background absorption band of the phosphate buffer at 1079 cm^{-1} (Figure 4C and ref *32*). However, histidine residues may also contribute here, and more detailed studies of this region are warranted. The 1505/1519 cm^{-1} peak/trough deserves mention since it is not consistent with the direction of redox shift observed in heme A model compounds (*26*). Changes in this region can arise from a ring-bending mode of tyrosine (*33*−*35*) and, therefore, might arise from the Y244 residue that is close to the heme a_3 and has been suggested to be of mechanistic importance in the reaction cycle (*36*, *37*).

Given the likelihood that the two copper centers lack contributions in the 1800−1000 cm^{-1} region apart from amide I/II contributions and, possibly, histidine vibrational changes, the majority of other features in the cyanide-ligated spectrum should arise solely from heme *a*. Again by comparison with Raman data, bands in the 1640−1600 cm^{-1} region are likely due to the ν(C═O) of the heme *a* formyl that is strongly downshifted due to strong hydrogen bonding and peaks and troughs in the 1585, 1520, 1238, and 1127 cm^{-1} regions are most likely due to heme *a* porphyrin. The more prominent amide I/II features reflect combined protein perturbations due to changes at both heme *a* and the copper centers. Another striking feature related to protein changes are the pair of troughs at 1748 and 1737 cm^{-1}. These are present in both the unligated and the cyanide-ligated redox difference spectra but are absent, or possibly replaced by a much weaker positive feature, in the double difference spectrum in Figure 6 that we attribute to the redox difference spectrum of heme a_3. These bands were also noted by Hellwig et al. (*17*) in their unligated redox spectrum and were attributed to changes of carboxylic acid residues based on assignments from studies on related oxidases (*12*−*15*). The data here show that these presumed carboxylic acid groups are changing in response to redox changes of Cu_A/heme a/Cu_B rather than heme a_3. The changes, which appear as troughs without associated peaks and in the simplest interpretation indicate deprotonation when Cu_A/heme a/Cu_B become reduced, may well be of key mechanistic significance, and we are now investigating them in more detail using mutant forms of yeast cytochrome *c* oxidase.

Comparison of the ATR and Transmission FTIR Techniques. The present data show that the ATR-FTIR technique can provide spectra comparable to those obtained by transmission FTIR. However, the ATR method offers several advantages for future studies. In the first instance, the amount of material required for comparable signals is 1−2 orders of magnitude less than that required for transmission FTIR. This makes feasible the study of enzymes that are difficult to purify in large amounts from various sources or as mutant forms. Second, the time taken to achieve stable baselines is far shorter, presumably due to the stability of the rewetted, thin layer of material, and the sample can be cycled repetitively through any ligand or reactant reaction. Both of these factors greatly facilitate acquisition of the high signal/noise that is required for analysis of spectra in terms of features of the protein and cofactors at the atomic level. The ATR method may prove particularly advantageous for probing the low-frequency (<1000 cm^{-1}) region where many important metal−ligand vibrations occur. By combination of appropriate prism material, optics, and detector, extension to at least 400 cm^{-1} is possible. Because the depth of penetration of the evanescent wave is inversely related to frequency (*18*), signals and signal/noise increase substantially and in a quantifiable manner as frequency decreases, as seen in Figure 3. In addition to these advantages, however, is the fact that the ATR-FTIR method allows study of a much greater range of possible transitions. In cytochrome *c* oxidase, this opens the way to FTIR analysis of ligand binding more generally, pH and redox titration, and conversion between reaction intermediates. By combination with flow-flash and time-resolved step-scan methods, the extension to analysis of the catalytic reaction cycle intermediates after reaction with oxygen may also now become feasible.

ACKNOWLEDGMENT

We are grateful to Jonathan Ramsey for technical assistance, to Santiago Garcia for electronic and mechanical assistance and to Dr. J. Ingledew for useful comments on the manuscript.

REFERENCES

1. Caughey, W. S., Dong, A., Sampath, V., Yoshikawa, S., and Zhao, X.-J. (1993) *J. Bioenerg. Biomembr. 25*, 81−91.
2. Alben, J. O., Moh, P. P., Fiamingo, F. G., and Altschuld, R. A. (1981) *Proc. Natl. Acad. Sci. U.S.A. 78*, 234−237.

3. Fiamingo, F. G., Altschuld, R. A., Moh, P. P., and Alben, J. O. (1982) *J. Biol. Chem. 257*, 1639−1650.
4. Einarsdóttir, O., Dyer, R. B., Lemon, D. D., Killough, P. M., Hubig, S. M., Atherton, S. J., López-Garriga, J. J., Palmer, G., and Woodruff, W. H. (1993) *Biochemistry 32*, 12013−12024.
5. Einarsdóttir, O., Choc, M. G., Weldon, S., and Caughey, W. S. (1988) *J. Biol. Chem. 263*, 13641−13654.
6. Park, S., Pan, L. P., Chan, S. I., and Alben, J. O. (1996) *Biophys. J. 71*, 1036−1047.
7. Mitchell, D. M., Shapleigh, J. P., Archer, A. M., Alben, J. O., and Gennis, R. B. (1996) *Biochemistry 35*, 9446−9450.
8. Puustinen, A., Bailey, J. A., Dyer, R. B., Mecklenburg, S. L., Wikström, M., and Woodruff, W. H. (1997) *Biochemistry 36*, 13195−13200.
9. Rost, B., Behr, J., Hellwig, P., Richter, O. M. H., Ludwig, B., Michel, H., and Mäntele, W. (1999) *Biochemistry 38*, 7565−7571.
10. Iwase, T., Varotsis, C., Shinzawa-Itoh, K., Yoshikawa, S., and Kitagawa, T. (1999) *J. Am. Chem. Soc. 121*, 1415−1416.
11. Tsubaki, M., and Yoshikawa, S. (1993) *Biochemistry 32*, 174−182.
12. Hellwig, P., Rost, B., Kaiser, U., Ostermeier, C., Michel, H., and Mäntele, W. (1996) *FEBS Lett. 385*, 53−57.
13. Lübben, M., and Gerwert, K. (1996) *FEBS Lett. 397*, 303−307.
14. Yamazaki, Y., Kandori, H., and Mogi, T. (1999) *J. Biochem.* (*Tokyo*) *126*, 194−199.
15. Lübben, M., Prutsch, A., Mamat, B., and Gerwert, K. (1999) *Biochemistry 38*, 2048−2056.
16. Hellwig, P., Behr, J., Ostermeier, C., Richter, O.-M. H., Pfitzner, U., Odenwald, A., Ludwig, B., Michel, H., and Mäntele, W. (1998) *Biochemistry 37*, 7390−7399.
17. Hellwig, P., Soulimane, T., Buse, G., and Mäntele, W. (1999) *FEBS Lett. 458*, 83−86.
18. Goormaghtigh, E., Raussens, V., and Ruysschaert, J.-M. (1999) *Biochim. Biophys. Acta 1422*, 105−185.
19. Moody, A. J., Cooper, C. E., and Rich, P. R. (1991) *Biochim. Biophys. Acta 1059*, 189−207.
20. Rich, P. R., and Moody, A. J. (1997) Cytochrome *c* oxidase, in *Bioelectrochemistry: principles and practice* (Gräber, P., and Milazzo, G., Eds.) pp 419−456, Birkhäuser Verlag AG, Basel, Switzerland.
21. Tsukihara, T., Aoyama, H., Yamashita, E., Tomizaki, T., Yamaguchi, H., Shinzawa-Itoh, K., Nakashima, R., Yaono, R., and Yoshikawa, S. (1995) *Science 269*, 1069−1074.
22. Rich, P. R., and Breton, J. (2001) *Biochemistry 40*, 6441−6449.
23. Moody, A. J., and Rich, P. R. (1990) *Biochim. Biophys. Acta 1015*, 205−215.
24. Hellwig, P., Grzybek, S., Behr, J., Michel, H., and Mäntele, W. (1999) *Biochemistry 38*, 1685−1694.
25. Heibel, G. E., Hildebrandt, P., Ludwig, B., Steinrücke, P., Soulimane, T., and Buse, G. (1993) *Biochemistry 32*, 10866−10877.
26. Han, S., Ching, Y., Hammes, S. L., and Rousseau, D. L. (1991) *Biophys. J. 60*, 45−52.
27. Choi, S., Lee, J. J., Wei, Y. H., and Spiro, T. G. (1983) *J. Am. Chem. Soc. 105*, 3692−3707.
28. Ching, Y., Argade, P. V., and Rousseau, D. L. (1985) *Biochemistry 24*, 4938−4946.
29. Argade, P. V., Ching, Y., and Rousseau, D. L. (1986) *Biophys. J. 50*, 613−620.
30. Behr, J., Hellwig, P., Mäntele, W., and Michel, H. (1998) *Biochemistry 37*, 7400−7406.
31. Rich, P. R., Meunier, B., Mitchell, R. M., and Moody, A. J. (1996) *Biochim. Biophys. Acta 1275*, 91−95.
32. Berthomieu, C., Boussac, A., Mäntele, W., Breton, J., and Nabedryk, E. (1992) *Biochemistry 31*, 11460−11471.
33. Venyaminov, S. Y., and Kalnin, N. N. (1990) *Biopolymers 30*, 1243−1257.
34. Dollinger, G., Eisenstein, L., Lin, S.-L., Nakashini, K., and Termini, J. (1986) *Biochemistry 25*, 6524−6533.
35. Hienerwadel, R., Boussac, A., Breton, J., and Berthomieu, C. (1996) *Biochemistry 35*, 15447−15460.
36. Gennis, R. B. (1998) *Biochim. Biophys. Acta 1365*, 241−248.
37. Proshlyakov, D. A., Pressler, M. A., and Babcock, G. T. (1998) *Proc. Natl. Acad. Sci. U.S.A. 95*, 8020−8025.

BI0109717